RSC Advances

ROYAL SOCIETY OF CHEMISTRY

www.rsc.org/advances

Pressure dependent Magnetic, AC Susceptibility and Electrical Properties of Nd_7Pd_3

Pramod Kumar,*[a] Puneet Jain[a] and Rachana Kumar[b]**

[a]*Magnetic and Spintronic Laboratory, Indian Institute of Information Technology Allahabad, Allahabad 211012, India,* *pkumar@iiita.ac.in;

[b]*National Physical Laboratory, New Delhi 110012, India,* **rachanak@nplindia.org

Abstract

Effects of pressure on magnetization and isothermal entropy change, AC susceptibility, and resistivity for Nd_7Pd_3 have been studied. Nd_7Pd_3 shows three magnetic transitions T_t (=15 K), T_C (=34 K), and T_N (=38 K) at a pressure of zero bar. T_C and T_N are very sensitive with pressure and rate of change of T_C and T_N with respect to pressure, i.e., dT_C/dp and dT_N/dp are -1.906 K/kbar and -0.313 K/kbar respectively, whereas T_t is insensitive to pressure change. It has also been observed that isothermal entropy change is also sensitive with pressure. Below 15 K, an indication of spin glass nature in ac susceptibility data is seen. Time dependent magnetization at low temperature also supports the spin glass nature but at high temperature it indicates the complex nature. Electrical resistivity data has been fitted to relation $\rho=\rho_0+AT^2$ in temperature range 12-30 K and $\rho=\rho_0+BT-CT^3$ in temperature range 40-220 K. M-H isotherm confirms the AFM nature of Nd_7Pd_3, confirmed further by Arrott's plot.

Introduction

The rare earth intermetallic compounds R_7M_3 (where R = rare earth metal and M = transition metal) have hexagonal Th_7Fe_3-type structure (space group: $P6_3mc$) [1]. R in this structure occupies three non-equivalent sites (6c, 12d and 2b) whereas M resides at the site 12b [2]. The compounds of this series have multiple magnetic transitions except Gd_7M_3[5]. As an example, Nd_7Rh_3 has two magnetic phase transitions at 34K and 9.1K [3], Sm_7Rh_3 has two transitions at 54 K and 25 K [4] and Gd_7Rh_3 behaves as an antiferromagnet below 150 K. In the same way, Nd_7Pd_3 behaves as an antiferromagnet to paramagnet at around 38 K [6], and a ferromagnet to antiferromagnet at a temperature of 34 K [6, 7].

Unlike, Nd_7Rh_3 which has the property to co-exist in antiferromagnetic and 'super-cooled' ferromagnetic phases after the reduction of magnetic field to zero, and still does not show spin-glass anomalies [8], Nd_7Pd_3 shows spin-glass nature at low temperature but does not co-exist in antiferromagnetic and 'super-cooled' nature [3]. In contrast to Gd_7Pd_3, which has spin dependent momentum density [9], Nd_7Pd_3 does not show this property, but Nd_7Pd_3 also has an interesting property that the FM→AFM (FM stands for ferromagnetism, AFM stands for antiferromagnetism), and AFM→PM (PM stands for paramagnetism) transition property of Nd_7Pd_3 is sensitive to pressure. Nd_7Pd_3 shows strong pressure effect as that is found in Ce_7Ni_3, where there is a transition from a magnetic state to a non-magnetic state takes place at low temperatures by applying weak pressure [6, 7]. Rare earth based intermetallic compounds (R_7M_3) have applications in magnetostriction, magnetoresistance and magnetocaloric effect [10, 11]. Magnetocaloric effect (MCE), which manifests as the heating or cooling of magnetic materials due to a varying magnetic field, has attracted considerable attention. The origin of MCE in many materials has been explained and its practical use to achieve low temperatures is being anticipated. Giant magnetocaloric effect exhibited by many rare earth (R)-transition metal (M) intermetallic compounds render them as potential refrigerants for magnetic refrigerators [10-11]. Large value of MCE spreads over a wide temperature range is considered as one of the most important requirements of a practical magnetic refrigerant system [10-11].

In this present work, we calculated the pressure effect on temperature dependent magnetization, and also on isothermal entropy change. It was shown by Sengupta et. al., [10] that in Nd_7Pd_3 there is an occurrence of kinetic hindrance, which leads to phase coexistence (supercooled ferromagnetic antiferromagnetic). They showed from the AC susceptibility data, that such a coexisting phase is different from spin. Nd_7Pd_3 shows spin glass so we have performed AC susceptibility and temperature dependent normalized magnetization data to confirm the spin glass nature in our sample. In the present work, we have also calculated the M-H isotherms and Arrott's

plot to study the magnetic structure of Nd_7Pd_3. Electrical resistivity measurements were also performed to study the metallic nature of this compound.

Experimental Details

The sample was prepared in an argon atmosphere using arc melting furnace. The starting materials were 99.8 % purity. The ingots were checked by X-ray diffraction after annealing at 873K for a week and found to be single phase (using the *fullProf* software) of Fe_7Th_3-type. The magnetization has been measured on different applied pressures (*P*) using a Cu–Be clamp type cell, which can work up to 12 kbar, attached to a SQUID magnetometer whereas ac susceptibility and transport in PPMS in the temperature range of 2–300 K. For the measurement of magnetization in a zero-field-cooled (ZFC) state, the sample was cooled from the paramagnetic state in a zero applied field, and the magnetization was measured while warming the sample. MCE has been calculated using M-H isotherms near transition temperature. Before measurement at each temperature the specimen was zero-field cooled from 60 K.

Results and Discussion

Figure 1 shows the room temperature powder X-ray diffraction pattern and Rietveld refinement of Nd_7Pd_3. All peaks can be indexed as the hexagonal Fe_7Th_3-type cell in the space group=$P6_3mc$ (a=10.1369(8) Å, b=10.1369(8) Å, c=6.38354(6) Å and $\gamma=120^0$). The sample is found to contain a small (2-3%) impurity of Nd_3Pd_2. The low values of R_P and R_B show that the pattern fitting is accurate [12] (shown in figure 1). The Bragg peaks of Nd_7Pd_3 (green line) and Nd_3Pd_2 (violet line) have also been shown in figure 1.

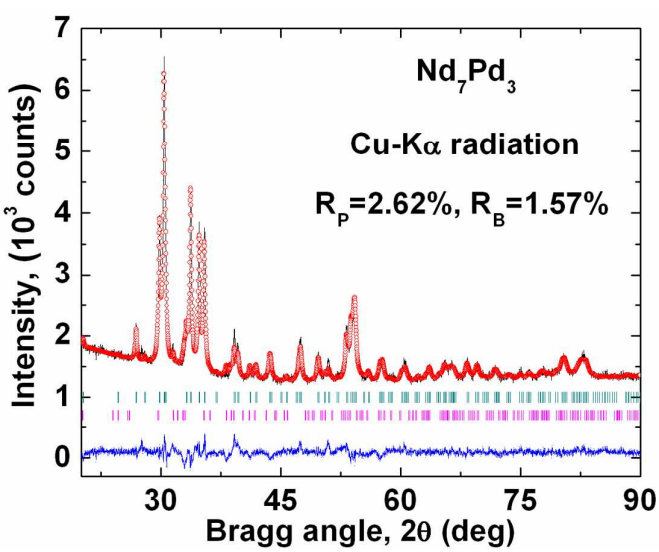

Figure 1: The observed (lines) and calculated (open circles) powder diffraction pattern of Nd_7Pd_3 after the completion of Rietveld refinement. The calculated positions of the Bragg peaks are shown as vertical bars [(Nd_7Pd_3 (green line) and Nd_3Pd_2 (violet line)] just below the plots of the observed and calculated intensities. The differences between the observed and calculated intensities are shown at the bottom of the plot.

Figure 2 shows the temperatue dependence of magnetization (M-T) in various applied pressure under field-cooled (FC), and zero-field-cooled (ZFC) modes, at 500 Oe. Figure 2(a) shows the M-T plot for FC condition. dM/dT v/s T plot clearly indicates three magnetic transitions at 15 K(=T_t), 34 K(=T_C) and 38 K(=T_N) as reported by Hideoki *et al.* [6]. While cooling down the sample, we get our first transition, around 38 K (at 0 bar) which is a paramagnetic (PM)→ antiferomagnetic (AFM) transition [6] and next transition at around T_C =34 K (at 0 bar) is AFM to ferromagnetic (FM). Below this at 34 K, Nd_7Pd_3 shows ferromagnetism, and around T_t of 15 K Nd_7Pd_3 shows another transition which is referred to as a glassy nature [6] which is due to magnetic frustation. As it is visible from figure 2(a), that as pressure is increased from 0 bar to 5 kbar (keeping H constant of 500 Oe), T_C decreases from 34 K to 15 K, and at high pressure of 9 kbar, T_N is dominating over T_C and T_t . So we can say that at 9 kbar, there is only PM→AFM transition, and there is no FM state [6]. Figure 2(a) clearly reveals that, as pressure is increased from 0 bar to 9 kbar, T_C and T_N shift towards a lower value, this is shown graphically by figures 2(c) and 2(d), that with increasing pressure, T_C and T_N decrease by the rate of dT_C/dp= -1.906 K/kbar and dT_N/dp= -0.313 K/kbar [6]. We have not plotted dT_t/dp as T_t is insensitive w.r.t pressure. Figure 2(b) shows the difference between ZFC and FC mode and this difference is decreasing with increasing pressure. We also observed with increasing pressure, diffrence is reduced, the reason being at high pressure T_N dominates over T_C and T_t.

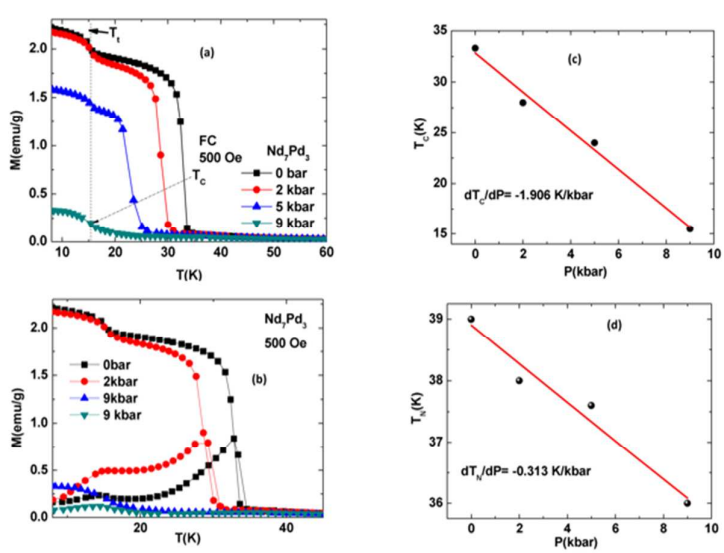

Figure 2: Magnetization v/s Temperature data of Nd_7Pd_3 (a) under FC and (b) ZFC and FC conditions obtained under various external pressures and in an applied field of 500 Oe. (c) T_c verses pressure and (d) T_N verses pressure plots of Nd_7Pd_3 compounds.

A question arises, whether the magnetic state attained after reversing the field to path zero is purely ferromagnetic in character. Figure 3(a) shows the isothermal magnetization behaviour of Nd_7Pd_3 at 28 K, 36 K, 38 K, 40 K, and 50 K. It can be noted from figure 3(a) that, at low field, there is some magnetization in Nd_7Pd_3, and this magnetization attains a saturation moment of 1.8 μ_B/Nd^{3+}[7]. This property of attaining maximum saturation at low magnetizing field indicates the ferromagnetic nature of Nd_7Pd_3 which is in agreement with figure 2(a). At high temperatures, there is a linear dependence of M on H, which accounts for the paramagnetic behaviour of Nd_7Pd_3 nature after the Neel temperatue. Figure 3(a) clearly reveals that as we go from 36 K to 38 K and then to 40 K, we are getting an off-axis M-H plots, and off-axis plot is a characterstic of antiferromagnetic materials, so we concluded that Nd_7Pd_3 is moving towards antiferromagnetic behaviour from ferromagnetic behaviour. To know the magnetic phase transition, we plot magnetization isotherms in the form of Arrott plot.

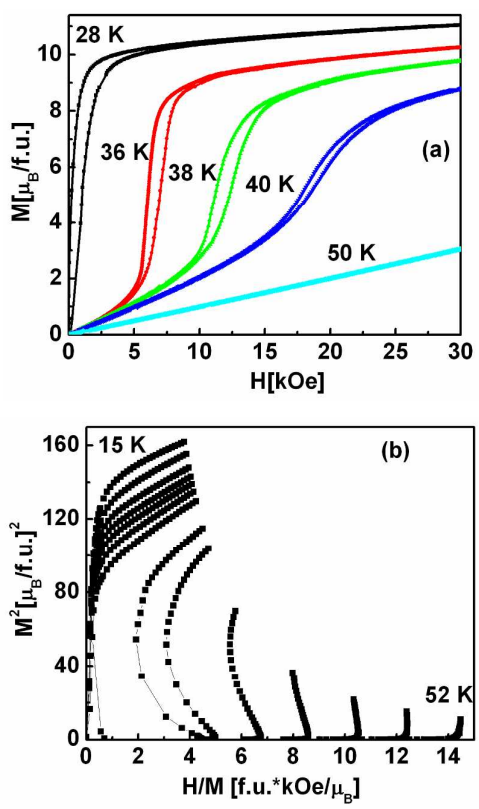

Figure 3: (a) M vs. H isotherms and (b) Arrott plots of Nd_7Pd_3 compound near ordering temperature. Before measurements at each temperature the specimen was zero-field cooled from 60 K.

Figure 3(b) shows the Arrott plots of Nd_7Pd_3. Arrott plots follow Landau expansion [13], where the mean free energy is given by

$$F(M) = \frac{aM^2}{2} + \frac{bM^4}{4} + ... - \mu_0 MH \cdots\cdots\cdots\cdots (1)$$

here, a and b are temperature dependent coefficients. However, Arrott plots can be used to estimate T_N in antiferromagnetic materials, and T_C in FM materials [14, 15] In the case of ferromagnetic and paramagnetic substances, b is positive, while a is positive for paramagnetic and negative for ferromagnetic materials. Banerjee [16] suggested that all Arrott plots with positive slope give second order magnetic phase transition while negative slope gives first order magnetic phase transition. A close view of figure 3(b) shows negative slope at low temperatures which indicates the first order magnetic phase transition at low temperature. We can see from this Arrott plot that as temperature is increased, we are getting antiferromagnetic behaviour. Also, at low temperatures we found that, Arrott plots are displaced to the left, which indicates the ferromagnetic behaviour. An S-shaped Arrott plots indicates FOT, which is depicted from 3(b).

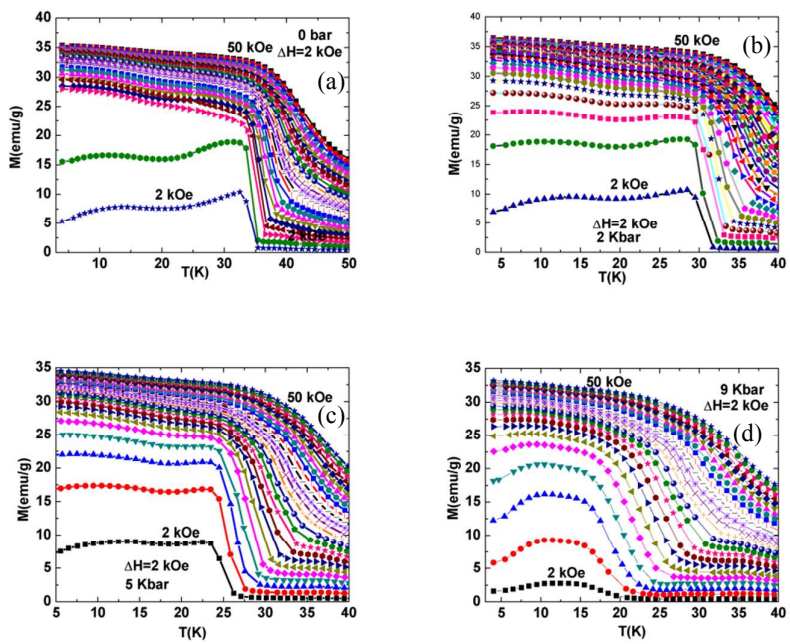

Figure 4: Temperature variation of magnetization on different field at (a) 0 bar, (b) 2 kbar, (c) 5 kbar and (d) 9 kbar.

Figure 4 shows the temperature variation of magnetization at different fields from 2 KOe to 50 KOe, with a gap of 2 KOe between every two successive fields, in ZFC mode. In figure 4(a) it has been found that at a pressure of 0 bar, we get a kink at around 15K, and at 34K, this matches with the date shown in figure 2(a) at 0 bar. Then as similar to figure 2(a), we get a downfall of magnetization

at around 38 K (=T_N). Figure 4(a) also reveals that as magnetic field is increase, T_N in increased. This same pattern is shown in figure 4(b), 4(c) and 4(d), and as pressure is increased, T_N is decreased.

Figure 4(b) shows temperature variation of magnetization on the same fields from 2 kOe to 50 kOe, but with a pressure of 2 kbar. So we can see here again T_t, T_C and T_N of 12 K, 28 K and 32 K, this data also coincides with magnetization v/s temperature data of figure 2(a). Similar are the results for figure 4(c) and 4(d). We also note a pattern here that as pressure increases from 0 bar to 9 Kbar, the magnetization decreases in value. At 9 Kbar, the FM state is again absent as can be seen from figure 4(d). Figure 4(d) also shows a huge broadening of the curves with increasing magnetic field, this is due to crystal anisotropy of Nd_7Pd_3.

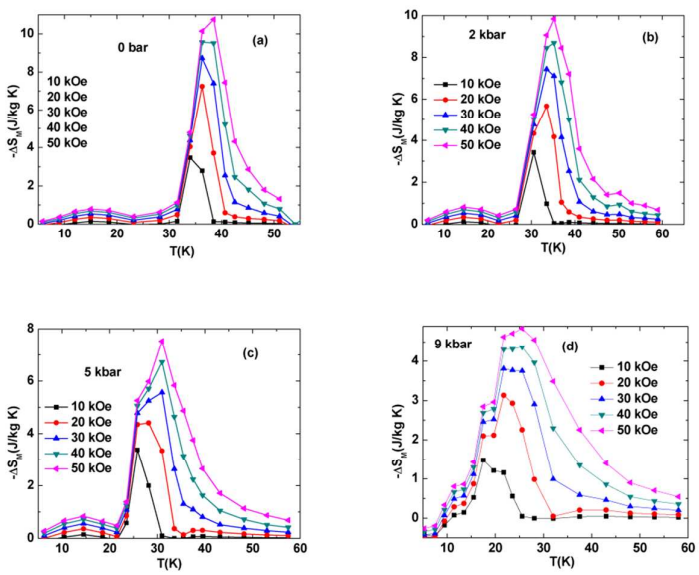

Figure 5: Temperature variation of isothermal entropy change (ΔS_M) in different fields at (a) 0 bar, (b) 2 Kbar, (c) 5 Kbar and (d) 9 Kbar.

Based on the magnetization isotherms measured near Curie temperature, the change in entropy of each sample near their ordering temperature was calculated using the integrated Maxwell relation [10-11]

$$\Delta S_M(T_{av}, H) = \int_{H_i}^{H_f} \left(\frac{\partial M}{\partial T}\right) dH \approx \frac{1}{\Delta T} \int_{H_i}^{H_f} \left[M(T_{i+1}, H_i) - M(T_i, H_f)\right] dH \quad (2)$$

Where $T_{av} = (T_{i+1}+T_i)/2$ means average temperature and $\Delta T = T_{i+1} - T_i$ means temperature difference between two magnetization isotherms measured at T_{i+1} and T_i with the magnetic field H_i to H_f. Figure 5 shows the MCE variation in Nd_7Pd_3 compound under various pressures. It can be seen from the figure that, with increase in pressure, the peak in the ΔS_M vs. T plot moves towards low temperatures. We note that Nd_7Pd_3 exhibits reversible magnetocaloric effect. In all the four graphs we can easily see

that the entropy change is negative (positive MCE). The maximum values of ΔS_M (ΔS_M^{Max}) are 3.8 J/kg K, 3.5 J/kg K, 3.1 J/kg K and 1.4 J/kg K at pressures of 0 bar, 2 Kbar, 5 Kbar and 9 Kbar respectively. At 0 bar, ΔS_M^{Max} is at T_N. Also, as the pressure is increased from 0 bar to 9 Kbar, the temperature at which, we get ΔS_M^{Max} gets reduced from 38 K to 28 K. A common pattern in all the four graphs of figure 5 is that, the magnitude of ΔS_M increases, as the value of applied field is increased from 10 KOe to 50 KOe, and as the pressure is increased from 0 bar to 9 Kbar, we get ΔS_M^{Max} at a lower temperature. To understand the magnetic structure, more studies like neutron diffraction, are required.

The AC magnetic susceptibility is magnetic susceptibility which we get by the application of AC magnetic field. AC susceptibility is written as

$$\chi_{ac} = \chi' - i\chi'' \ldots\ldots\ldots\ldots (3)$$

In equation (3), χ' and χ'' refers to the real and imaginary component of the AC susceptibility. Real component is also called the in-phase component and imaginary component is also called the out-of phase component. AC susceptibility is used to study the magnetic phase transition [17]. From figure 6(a), we can see three transitions in the real component, where the first peak is around 15 K, which corresponds to the transition temperature, T_t as shown in figure 2(a). Another similarity between figure 6(a) and 2(a) is that in 6(a) there is another peak at around 34 K. This can be viewed by taking figure 6(b) into consideration. If in AC susceptibility of a sample, there is a peak in χ' at a temperature, and for the same temperature there is a non-zero χ'', then it means the sample is ferromagnetic. This is what is being indicated by figure 6(a) and 6(b), for the peak around 34 K, which is nothing but the T_C, so we can say 34 K is the Curie tempearute of the Nd_7Pd_3. Similarly we get a peak in figure 6(a) at 38K, which corresponds to the Neel temperature of Nd_7Pd_3. For a sample to be antiferromagnetic, there is a peak in χ' at a temperature, and for the same temperature there is a zero χ''. This is what shown by figure 6(a) and 6(b), but as the frequency of the AC field increases, the AFM nature becomes reduced. In figure 6(b), there is a strong frequency dependence of AC susceptibility at low temperature (i.e. below 15K) which is a clear indication of magnetic glassy state. The χ'' v/s T plot tells that at T_f, there is a strong peak, but at higher temperatures, χ'' is nearly equal to zero, but it has a non-zero value below T_f. This is a characteristic of spin glass transition [17]. To understand the glassy nature at low temperature, we analyzed frequency dependent Vogel-Fulcher law and time dependent magnetization fitting.

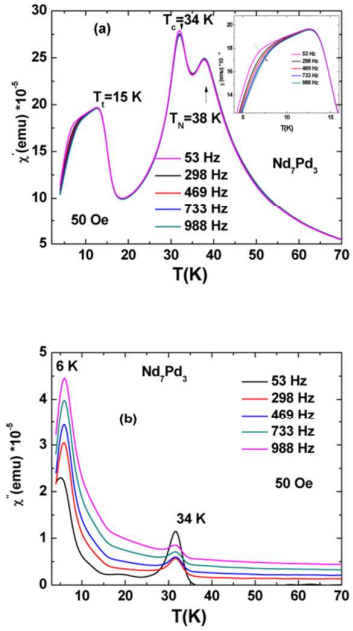

Figure 6: Temperature variation of the (a) real and (b) imaginary component of the ac magnetic susceptibility of Nd_7Pd_3 in a 5Oe AC magnetic field at various frequencies.

The glassy nature as stated in figure 6(b) is analyzed using empirical Vogel–Fulcher (VF) power law and is shown in figure 7, which shows the variation of spin freezing temperature T_f with relaxation time T_0. The AC susceptibility fits well with power law

$$T_f = T_0 + [(E_a / \kappa_B)/100]X \text{ ..... } (4)$$

where, T_0 is given by 1.54K, E_a is activation energy, κ_B is Boltzman constant, and $E_a / \kappa_B = 14.95K$. As can be seen from figure 7, T_f increase linearly with an increase with the logarithmic plot of ω_0/ω, where ω_0 is the attempt frequency ($\omega_0 = \frac{1}{T_0}$) and ω is the operating frequency.

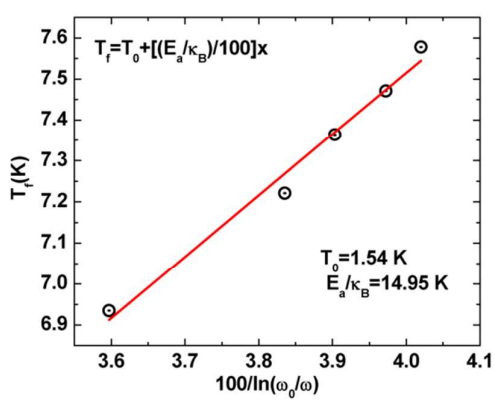

Figure 7: Frequency dependent temperature data fiited using the empirical Vogel-Fulcher law below T_t.

Figure 8, shows normalized magnetization, M as a function of time at various temperatures in ZFC mode. M_0 is the magnetization at t = 0. All the measured values of M are normalized w.r.t M_0.

Figure 8(b) shows, normalized magnetization with time as varying function, at 3 K, and it has been found that at 3 K, the magnetization is explained using combination of two laws named as power law and stretched exponential law, given by

$$M(t)/M0 = P1*(1-2*t^{\gamma}) + P2*\exp((-t/\tau)^{\beta}) \quad (5)$$

here, P1 and P2 are temperature dependent weight factors for both the power law and stretched exponential respectively. The stretched law is a characteristic associated with spin glass nature, so stretched law in equation 5 indicates the glassy nature of Nd_7Pd_3 at low temperature. But as there is also a contribution of power law in equation 5, which signifies that glassy nature has not completely formed.

Figure 8(c) shows that at 25K, normalized magnetization, M, is very well fitted with the power law

$$M/M(0) = -1 + 2t^{\gamma} \ldots\ldots (6)$$

In figure 8(c) the red solid line is fit to the data using power law [18]. As at 25K, normalized magnetization obeys power law, which tells about the metastability across the FOT, similar to solidification of melt when melt is undercooled. We are not able to fit in equation (6) or (7), the other temperatures. It is a clear indication of complex magnetic structure at high temperature.

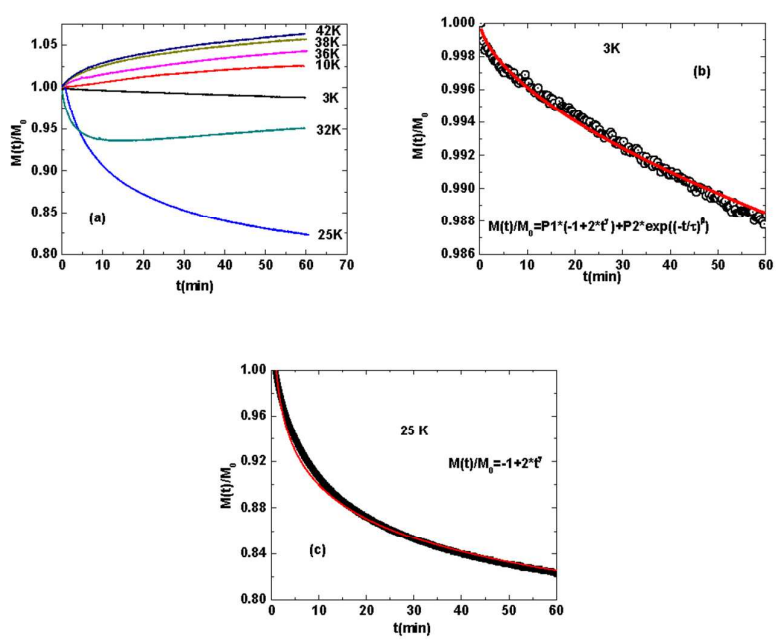

Figure 8: (a) Normalized magnetization vs time (t) plot for Nd_7Pd_3 compound measured at different temperature an applied field of 10 kOe in the virgin H cycle. For each H, M(0) is the value of the magnetization recorded when relaxation measurement were started. (b) At 3K data fitted with equation $M/M(0) = Pl(-1+2t^{\gamma}) + P2*\exp((-t/\tau)^{\beta})$ *(c) At 25 K data fitted with equation* $M/M(0) = -1+2t^{\gamma}$.

To get a better insight into the magnetic state of the compound, measurements on electrical resistivity were carried out. Figure 9 shows the electrical resistivity of Nd_7Pd_3 as a function of temperature. From 9(a), we found that the residual resistivity of the sample is about 0.01 mμ-cm. Nd_7Pd_3 showing metallic character. There is a change in slope of the resistivity near all the magnetic transition as given in figure 2(a). Figure 9(a) shows three transitions. It can be found that at low temperature (i.e. temperature below T_C) resistivity follows the equation $\rho=\rho_0+AT^2$ and at high temperatures (i.e. temperature above T_N) resistivity follows $\rho=\rho_0+BT-CT^3$, where ρ_0 is residual resistivity [9] given by 8.67E-6Ω-cm at low temperatures and 6.91E-5Ω-cm at high temperature respectively. A, B and C are temperature independent constants [9, 19]. From the electrical resistivity, we can conclude that Nd_7Pd_3 is metallic in nature over the entire temperature range, and because of the loss of spin disorder scattering due to spontaneous magnetic ordering, there is a drop in resistivity at T_C=34 K.

The second term in $\rho=\rho_0+AT^2$ is proportional to T^2 and represents the lattice spin waves. For figure 9(b), A=5.8E-8 Ω-cm/K^2 and suggests that electron spin-wave scattering is dominant factor that helps to determine electrical resistivity in the temperature range of 12-32 K. Similarly, in high temperature range, $\rho=\rho_0+BT-CT^3$, B=4.58E-7 Ω-cm/K and C=2.37E-12 Ω-cm/K^2 indicates the phonon contribution and also indicates that s-d scattering [9] is important in high temperature range i.e. above 40 K. Figure 9(b) and 9(c), are plotted, to determine the dominant contributions in the electrical resistivity data [20].

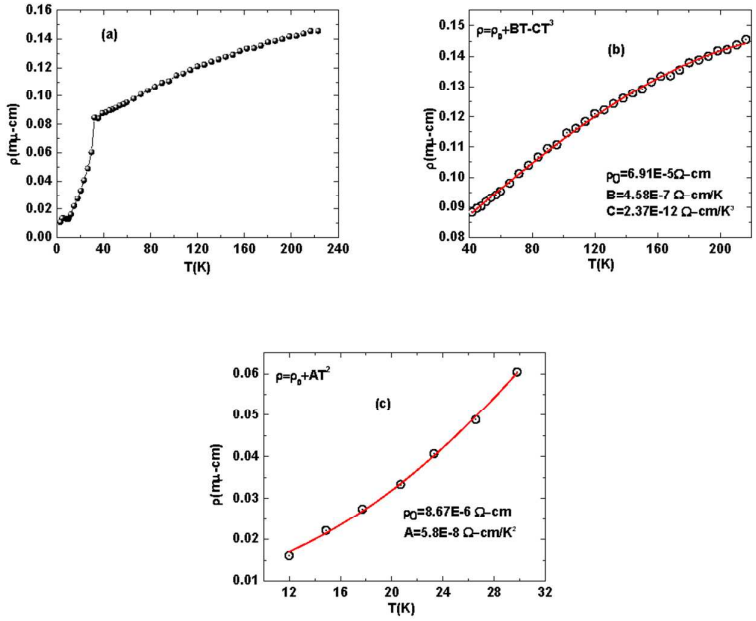

Figure 9: (a) Temperature dependent of electrical resistivity of Nd7Pd3 compound. Electrical resistivity data fitted to relation (b) $\rho=\rho_0+AT^2$ in temperature range 12-30 K (b) $\rho=\rho_0+BT-CT^3$ in temperature range 40-220 K.

Conclusions

Electrical resistivity, AC susceptibility, MCE and magnetization measurements were performed on Nd_7Pd_3 showing three magnetic transitions, first at around 15 K, then second at around 34 K and the third is around 38 K where, 34 K and 38 K are the Curie temperature and Neel temperature of Nd_7Pd_3 respectively. For a field of 10 kOe, it showed a MCE of 3.8 J/kg K, at 0 bar. The calculated values of T_C and T_N match with M-H isotherm, AC susceptibility and temperature dependent electrical resistivity as well. Spin glass nature has also been confirmed by temperature dependent AC susceptibility, normalized time dependent magneitzation and Vogel-Fulcher law. The χ'' v/s T plot tells that at T_f, there is a strong peak, but at higher temperatures, χ'' is nearly equal to zero, but it has a non-zero value below T_f. This is a characteristic of spin glass transition. Electrical resistivity of Nd_7Pd_3 as a function of temperature tells that Nd_7Pd_3 has metallic nature over the entire temperature range, and because there is a loss of spin disorder scattering, there is a drop in resistivity at T_C=34 K. M-H isotherm and Arrot's plots show the AFM nature of Nd_7Pd_3,, which is in accordance with M-T

data in FC mode. M-T data at various pressures and at constant field of 50KOe confirms the magnetic ansiotropy of Nd7Pd3. This data has been verified by MCE plots. Large refrigerating cooling power, large isothermal entropy change, soft magnetic behaviour and wide operating temperature range make it an attractive candidate as magnetic refrigerant in low temperature region.

Acknowledgement

One of the authors (Pramod Kumar) thanks DST, Govt. of India for proving financial support for this work. We would like to thank Dr. Alexandre Carvalho and Prof. Gamma for helping us in high pressure measurements.

References

1. T. Matsushita, K. Shimonura and T. Tsutaoka, *J. Korean Phys. Society*, 2013, **63**, 559-562.
2. S. Rayaprol, V. Siruguri, A. Hoser, P. Henry and E. V. Sampathkumaran, *J. Phys.: Conference Series*, 2012, **340**, 012064.
3. A. Tanaka, T. Tsutaoka and T. Shigeoka, *Physica B: Cond. Matter*, 2008, **403,** 3248–3254.
4. T. Tsutaoka, D. Noguchi, Y. Nakamori, G. Nakamoto and M. Kurisu, *Physica B: Cond. Matter*, 2013, **426**, 108-111.
5. K. Sengupta, S. Rayaprol and E.V. Sampathkumaran, *arXiv: cond-mat/0411608*.
6. H. Kadomatsu, K. Kuwano, K. Umeo, Y. Itoh and T. Tokunaga, *J. Magn. Magn. Matter.,* 1998, **189**, 335-340.
7. N. K. Singh, P. Kumar, Z. Mao, D. Paudyal, V. Neu, K. G. Suresh, V. K. Pecharsky and K. A. Geschneider, *J. Phys. Conds. Matter*, 2009, **21**, 456004-456008.
8. K. Sengupta and E. V. Sampathkumaran, *J. Phys.: Cond. Matter*, 2006, **18**, 401-406.
9. C. Shenton Taylor, J. A. Duffy, J. W. Taylor, C. A. Steer, D. N. Timms, M. J. Cooper and L. V. Blaauw, *J. Phys.: Condens. Matter*, 2007, **19**, 186208.
10. D. Gignoux and D. Schmitt *J. Magn. Magn. Matter.,* 1991, **100**, 99-125.; P. Kumar, N. K. Singh, K. G. Suresh, A. K. Nigam and S. K. Malik, *J. Appl. Phys.*, 2007, **101**, 013908.; P. Kumar, N. K. Singh, K. G. Suresh, A. K. Nigam, *J. Alloys Comp.*, 2007, **427**, 42; K. Sengupta and E.V. Sampathkumaran, *arXiv: cond-mat/0512542.*
11. P. Kumar, N. Singh, K.G. Suresh and A.K. Nigam *Phys. Rev. B,* 2008, **77**, 184411.; P. Kumar, N. K. Singh, K. G. Suresh and A. K. Nigam, *J. Phys.: Condens. Matter*, 2007, **19**, 386210.; N.

K. Singh, P. Kumar, K. G. Suresh and A. K. Nigam, *J. Phys.: Condens. Matter*, 2007, **19**, 036213.

12. S.-Heon, S. J. Kim and J. Ho, *American Mineralogist,* 1996, **81**, 1133-1140.
13. Magnetism, Volume 1 edited by Etienne Du Trémolet de Lacheisserie, D. Gignoux, Michel Schlenke 2002 (Springer USA).
14. P. J. Webster and K. R. A. Ziebeck, Heusler Alloys, in Magnetic Properties of Metals, Landolt-Bornstein New Series Group III, edited by H. R. J. Wijn (Springer, Berlin),1988, **19C,** 75.
15. C. Kittel, Introduction to Solid State Physics (John Wiley Sons, New York), 1976.
16. S. K. Banerjee, *Phys. Lett*., 1964, **12**, 16-17.
17. T. Chakrabarty, A. V. Mahajan and S. Kundu, *J. Phys.: Condens. Matter*, 2014, **26,** 405601; S. Chatterjee, S. Giri, S. K. De and S. Majumdar, *Phys. Rev. B* 2009, **79**, 092410; E. Obrado, A. Planes, B. Martinez, *Phys. Rev. B,* 1999, **59**, 11450; F. Wang, J. Zhang, Y.-fu Chen, G.-jun Wang, J-rong Sun, S.-ying Zhang and B.-gen Shen, *Phys. Rev. B* 204**, 69**, 094424; E. M. Levin, V. K. Pecharsky and K. A. Gschneidner Jr., *J. of Appl. Phys.* 2001, **90**, 6255; R. Mahendiran, Y. Breard, M. Hervieu, B. Raveau and P. Schiffer, *Phys. Rev. B* 2003, **68,** 104402; M. K. Singh, W. Prellier, M. P. Singh, R. S. Katiyar and J. F. Scott, *Phys. Rev. B* 2008, **77**, 144403; Q. Luo, D. Q. Zhao, M. X. Pan and W. H. Wang, *Appl. Phys. Lett*. 2008, **92**, 011923; M. Viswanathan and P. S. Anil Kumar, *Phys. Rev. B* 2009, **80**, 012410; N. Hanasaki, K. Watanabe, T. Ohtsuka, I. Kezsmarki, S. Iguchi, S. Miyasaka, and Y. Tokura, *Phys. Rev. Lett*. 2007, **99**, 086401.
18. M. Manekar, M. K. Chattopadhyay and S. B. Roy, *J. Phys: Condens. Matter*, 2011, **23**, 086001-086006.
19. K. G. Suresh and K. V. S. Rama Rao, *J. Alloys Compd*. 1996, **238**, 90-94.
20. S. Gupta, K.G. Suresh and A. K. Nigam. *arXiv: 1302.4226v2.*